SolarPACES 2022, 28th International Conference on Concentrating Solar Power and Chemical Energy Systems
Receivers and Heat Transfer Media and Transport: Point Focus Systems
https://doi.org/10.52825/solarpaces.v1i.718

Published: 19 Feb. 2024

# Discrete Element Method Modelling of the Particle Flow in Centrifugal Solar Particle Receiver

Serdar Hicdurmaz[1,3][https://orcid.org/0000-0002-4080-5693], Reiner Buck[1][https://orcid.org/0000-0002-3821-9409], and Bernhard Hoffschmidt[2,3][https://orcid.org/0000-0003-4068-2053]

[1] German Aerospace Center (DLR), Institute of Solar Research, Germany

[2] German Aerospace Center (DLR), Institute of Solar Research, Germany

[3] RWTH Aachen University, Chair of Solar Components, Germany

**Abstract.** The centrifugal solar particle receiver (CentRec) is a promising design compared to other particle receiver concepts because it allows for an active adjustment of particle residence time and particle outlet temperature by adjusting the rotational speed of the drum and particle mass flow rate. A Discrete Element Method (DEM) tool is utilized to model the particle flow in CentRec. However, the numerical modeling of the particle flow in large scale receiver is computationally infeasible because of excessive number of particles in the simulation. Thus, in this study, a scale down approach is developed and validated to be used to estimate the particle film characteristics in large scale receivers. The particle velocity profile and film thickness distribution are employed to compare different receiver sizes.

**Keywords:** Particle Receivers, Discrete Element Method, Concentrating Solar Power, Centrifugal Solar Particle Receiver

## 1. Introduction

Particle solar receivers promise higher thermal efficiency and lower operational and component cost compared to molten salt based solar receivers in solar tower applications. The centrifugal solar particle receiver (CentRec) is a direct absorption receiver concept where the ceramic particles descend through the inclined rotating drum while being exposed to the solar beams concentrated by the heliostat field [1]. The Discrete Element Method (DEM) is used to model the motion of the discrete particles in the receiver to obtain the flow characteristics. Previous efforts have been put on the thermal model development of the particle flow in CentRec [2, 3], but the number of particles in the simulation of a large-scale receiver (cavity diameter > 1 meter) is hundred-millions, which is computationally infeasible to simulate. Thus, scaling down of the receiver while keeping the particle flow characteristics the same is addressed in this study.

## 2. Model Details

The open source DEM tool “LIGGGHTS” is employed to simulate the particle motion in CentRec. Particles are assumed as spheres and monodispersed. Sintered bauxite particles (SG 16/30) with mean Sauter dimeter of 1.2 mm are considered [4]. In DEM, the net force acting on each particle is calculated, and the particle motion is found by Newton’s laws of motion for every DEM time step. The main forces on a particle are the normal and tangential forces exerted by other particles being in contact with, fluid forces and gravity. However, in this study the fluid part filling the voids between moving particles is not modelled because the drag force

exerted by the fluid is much smaller than gravity and particle interaction forces in CentRec application. This assumption may not be valid if strong fluid forces like wind exist. The fluid motion due to temperature and density gradients in the fluid phase within the particle film is also negligible compared to interparticle forces and gravity. Thus, the velocity field of particle and fluid phase can be assumed as same to each other. The built-in contact force models being available in LIGGGHTS v3 [5] are considered in this study. The Hertzian normal and tangential force models with history effect are employed. In Hertzian model, the contact is modelled as a spring-dashpot mechanism, in which stiffness and damping coefficients are function of the particle overlap. In order to able to capture the particle contact in a larger time step, particles are artificially softened, and the normal and tangential forces are formulated as a function of normal and tangential overlap, respectively. This “soft sphere” approach is commonly used in DEM simulations to reduce the computational time. The rolling resistance model accounting for the non-spherical shape of the realistic particles is chosen as “epsd2” model. By applying this model, a fictitious torque is applied to spherical particle in reverse rolling direction. The model equations are not discussed here for brevity and can be found in [4-6].

The particle properties considered in the simulation are listed in Table 1. Three DEM particle properties have already been calibrated by particle experiments in previous studies. The sliding and rolling friction coefficients are calibrated by using the CentRec experiments [6] whereas the restitution coefficient is found by a plate impact experiment [7] for SG 16/30 particles.

**Table 1.** DEM input parameters for particles.

| | | |
|---|---|---|
| Sauter Diameter | mm | 1.2 |
| Density | kg/m$^3$ | 3560 |
| Young's Modulus | MPa | 5 |
| Poisson's Ratio | - | 0.3 |
| Sliding Friction Coefficient | - | 0.81 |
| Rolling Friction Coefficient | - | 0.26 |
| Restitution Coefficient | - | 0.46 |

## 3. Scale down approach

The new approach to scale-down the particle film assumes that if the net force acting on a particle film during the particles’ residence time is the same, the velocity field is also the same regardless of the receiver size. There are two major forces acting on the particle film. The first one is the gravity, being independent of all operational parameters. The second is the fictitious centrifugal force, which is not a real force but an effect that a matter experiences during the circular motion, that pushes the matter outward of the circular path. The friction force is a result of various combinations of these two forces during the motion. Gravity is assumed to be the same for all particles regardless of the receiver size. In order to also apply the same centrifugal force to the moving film, the rotational speed must be adjusted as follows.

$$w_{act}^2 r_{act} = w_{sim}^2 r_{sim} \quad (1)$$

The actual and simulation rotational speed are denoted as $w_{act}$ and $w_{sim}$, respectively. Similarly, the cavity radius is denoted as $r_{act}$ and $r_{sim}$. The scale-down approach is valid if the cavity diameter is much higher than the particle diameter so that the cavity wall can be assumed as flat relative to the single particle. To obtain the same film thickness, the mass flow rate also needs to be adjusted.

$$\frac{\dot{m}_{act}}{r_{act}} = \frac{\dot{m}_{sim}}{r_{sim}} \tag{2}$$

The cavity length is also adjusted to have the same aspect ratio (cavity length/diameter).

$$\frac{L_{act}}{r_{act}} = \frac{L_{sim}}{r_{sim}} \tag{3}$$

## 4. Results

The scale-down approach claims that by applying the three scaling laws, one can obtain the same velocity and film thickness distribution along the receiver. In the DEM simulations, particles are introduced into the domain at the axial top of the inclined receiver with a linear velocity being the same as the cavity wall's linear velocity and zero axial velocity, as seen in Figure 1(a). The radial location of particle generation domain is 10 $d_p$ (particle diameter) away from the cavity wall, as depicted in Figure 1(b). The receiver tilt angle is set to 45°, as seen in Figure 1(c), throughout the study.

In order to check the applicability of the new approach to CentRec, three receiver sizes are considered, as shown in Table 2. The particle diameter for all sizes is 1.2 mm so the cavity diameter is 100 times $d_p$ for the smallest receiver size.

The particle – surface friction coefficient is set to very high value (10,000) so that the particles touching the cavity wall do not move relative to the wall. This numerical trick is done to obtain a stationary particle layer at the wall like in the real operation [8]. In Figure 2, the particle mass flow rate at the outlet of the receiver is plotted for all sizes. As can be noticed, after a certain period of time, the mean outlet mass flow rate is equal to inlet mass flow rate; however, there is a certain level of the fluctuations around the mean value. The fluctuations at the outlet may indicate that the film thickness changes periodically because the instantaneous number of particles in the receiver also changes with time slightly. During the initial filling period, there is quite large particle loss through the aperture. This is mainly because the wire mesh structure, which is considered in the real application to obtain a stationary particle layer on the cylindrical cavity wall, is not modelled in the CAD model of the receiver. This transient effect is not the representation of the reality and only occurs due to implicit modelling of the wire mesh.

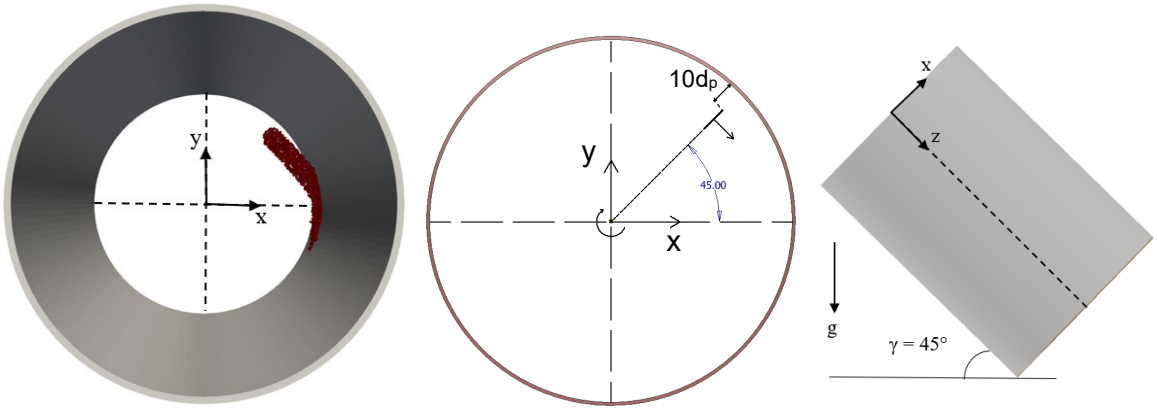


**(a)** **(b)** **(c)**

**Figure 1**. (a) Feeding of the particles to the cavity (b) Location of particle feeder (c) Side view of the tilted receiver.

**Table 2.** Receiver dimensions considered in scaled-down approach.

| | Unit | D12 | D17 | D25 |
|---|---|---|---|---|
| Cavity Diameter | m | 0.12 | 0.17 | 0.25 |
| Cavity Length | m | 0.171 | 0.242 | 0.356 |
| Mass Flow Rate | g/s | 35.7 | 50.58 | 74.38 |
| Rotational Speed | rpm | 160.08 | 134.50 | 110.91 |
| Particle Inlet Speed | m/s | 1.01 | 1.20 | 1.45 |
| Particle number in the simulation (x$10^5$) | - | 1.6 | 3.3 | 7 |

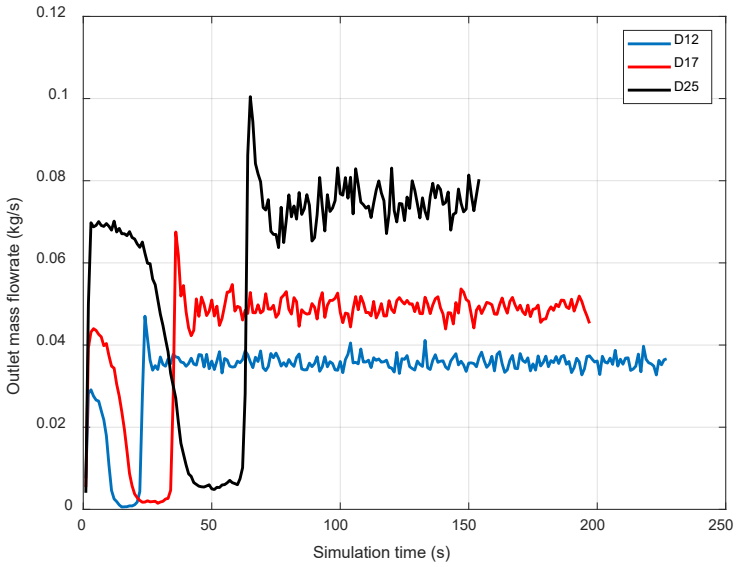


**Figure 2**. Time variation of particle outlet mass flow rate for three receiver sizes.

After obtaining the cold steady state, meaning that the inlet and outlet mass flow rate are equal to each other, the velocity and film thickness distribution for the three sizes are compared. The film thickness for any axial segment of the particle film is calculated by averaging the radial position of the particles located at the particle film surface. Firstly, the surface area of the axially-cut film section is calculated.

$$A_{surf} = l_{sec}\pi(d_{cav} - 2t_{film}) \tag{4}$$

The axial length of the film section is denoted as $l_{sec}$ while the film thickness is denoted as $t_{film}$. Because the surface area is also function of film thickness, the calculation of the film thickness requires the iterative solution. Then, the number of particles forming the particle film surface is calculated as

$$n_p = \frac{A_{surf} d_p (1 - f_s)}{V_p} \tag{5}$$

Particle diameter, particle volume and bulk solid fraction are denoted as $d_p$, $V_p$ and $f_s$. For the particle type considered in this study and the relevant operational range, the solid fraction is found as 0.5 ± 0.02 in the CentRec simulations [6]. Thus, an average value of 0.5 is assumed in this calculation. Note that in Eq. (5), it is assumed that the particles forming the film section are evenly distributed in tangential and axial directions, i. e. there is no pile formation. Later, the radial position of all particles in the enclosed hollow cylinder-like volume is found by using

the particles' x and y positions. Then, particles are sorted by their radial positions in ascending order, and a sorted radial position vector "$r_p$" is formed.

$$r_p = sort(\sqrt{x_p^2 + y_p^2}, 'ascend') \tag{6}$$

The first $n_p$ elements of vector $r_p$ correspond to the particles forming the particle film surface. Then, the film thickness for a given axially-cut section of the film is found as follows.

$$t_{film} = \frac{d_{cav}}{2} - \frac{\sum_{i=1}^{n_p} r_p[i]}{n_p} + \frac{d_p}{2} \tag{7}$$

In Eq. (7), the average radial position of $n_p$ particles being farthest from the wall is subtracted from the cavity radius. Moreover, the particle radius should be added because the radial position of a particle is defined as the distance between the particle center and cavity centerline. However, the film thickness is defined as the distance between cavity wall and the tip of the spherical cap of the particle. Eqs. (4) – (7) are solved iteratively with an initial guess for $t_{film}$. Assuming that the film thickness is zero in Eq. (4) in the first iteration is enough for the convergence in this study.

In Figure 3, the tangentially averaged film thickness in the axial direction for three receiver sizes is plotted. The trend of film thickness for three receiver sizes is quite similar with the largest deviation of $0.1d_p$. For all sizes, the film thickness is getting smaller near the exit. For the considered rotational speed and mass flow rate couples, the change in the film thickness in the axial direction is not large. There is also a slight difference in the film thickness in tangential direction. The porosity of the film is ~ 0.48 in the stationary zone while it is ~0.52 in the moving zone. Due to continuity, there is ~8% difference between film thicknesses of the two zones for the considered operational parameter set.

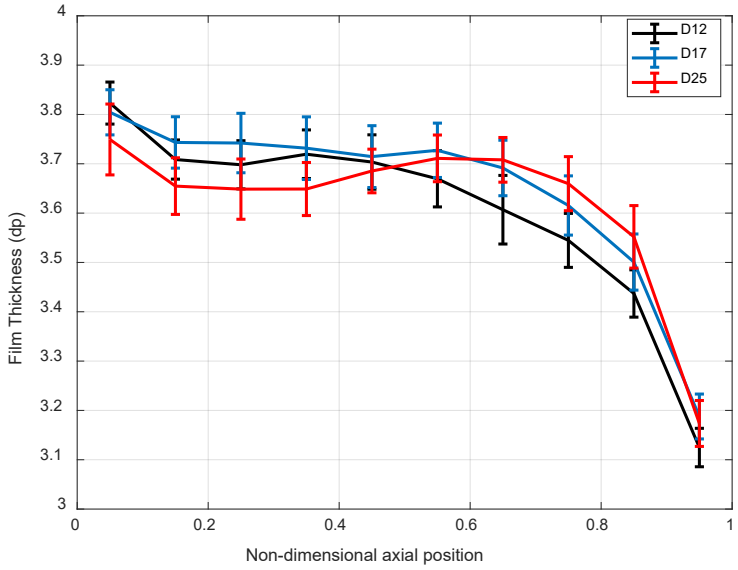


**Figure 3**. Tangentially averaged film thickness averaged for 150 turns. The error bar is the mean standard deviation. 0 and 1 in x axis correspond to inlet and exit of the receiver.

In Figure 4, the axial velocities of the particles in three receiver sizes are qualitatively compared by representing receivers in concentric manner. The rotation direction is clockwise, as depicted in Figure 1(b). The moving and stationary zones are noticeable. The angular positions where

the stationary zone starts and ends are quite similar for all sizes. Moreover, the axial velocity profiles on the surface in the moving zone are also similar. In order to compare the velocity profiles quantitatively and in deeper parts of the particle film, nine combinations of three different tangential and axial positions are determined as shown in Figure 5. In each arc-like particle film sections, the axial velocity profiles in radial direction are determined by averaging the results for 150 turns. In Figure 6 (a)-(c), the axial velocity profiles in the radial direction at nondimensional axial position of z = 0.3 are presented for three different tangential positions located in the moving zone. The profiles for the sizes D12 and D25 match very well in all tangential positions; however, there are slightly lower velocities for D17 at 90° and 135°. This is probably due to that the film thickness at z = 0.3 for D17 is slightly higher, as can also be noticed in Figure 3. Similar deviations are also observed for D25 at 45° and z = 0.5 in Figure 6 (d), for D12 at 45° in Figure 6 (g) and D17 at 135° in Figure (i). However, in general, there is a very good agreement between particle velocity profiles up to the calculated film thickness. There is no detectable trend for the particles whose centers are beyond ~4.5 $d_p$ for 45° and 90°, and beyond ~4 $d_p$ for 135°. These particles being located on the surface of the film probably move freely or collide with several particles in the moving zone while being exposed to less amount of the friction force. Thus, their motion is not representative for the flow behavior. Note that each circle in these figures corresponds to the average velocity of the particles in the representative location so the figures do not show the particle density in the radial direction.

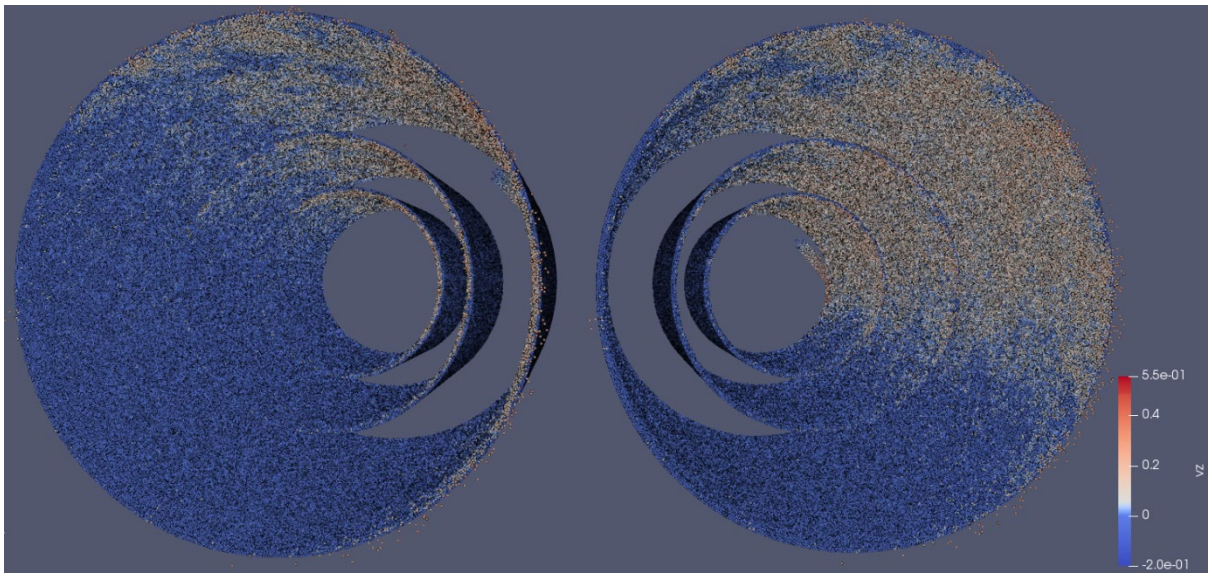


**(a)** **(b)**

**Figure 4**. Qualitative comparison of axial velocities for three receiver sizes. A view of (a) stationary zone (b) moving zone. The color bar is the axial velocity in m/s.

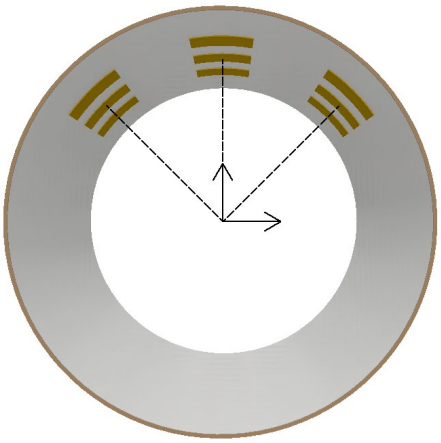

**Figure 5**. The arc-like section volumes to be used in the determination of the velocity profiles. The tangential positions of volumes are 45°, 90° and 135° in counter clockwise direction. The non-dimensional axial positions are 0.3, 0.5 and 0.7.

In the velocity profile figures, it can also be noticed that the axial velocity profile in the radial direction follows a nearly linear trend from 1 $d_p$ to the film thickness value for all cases. Because the stationary particles do not move relative to the wall, the axial velocity is always zero for $r_p$ < 1$d_p$ region. In Figure 6 (a), the data points are fitted by a linear curve between 1$d_p$ and 4$d_p$. Although there is hump-like shape in the velocity profile due to particle layering effect resulting from the existence of the wall, the linear velocity profile assumption may be useful for further scaling-up of the CentRec but this is out of the scope of this study.

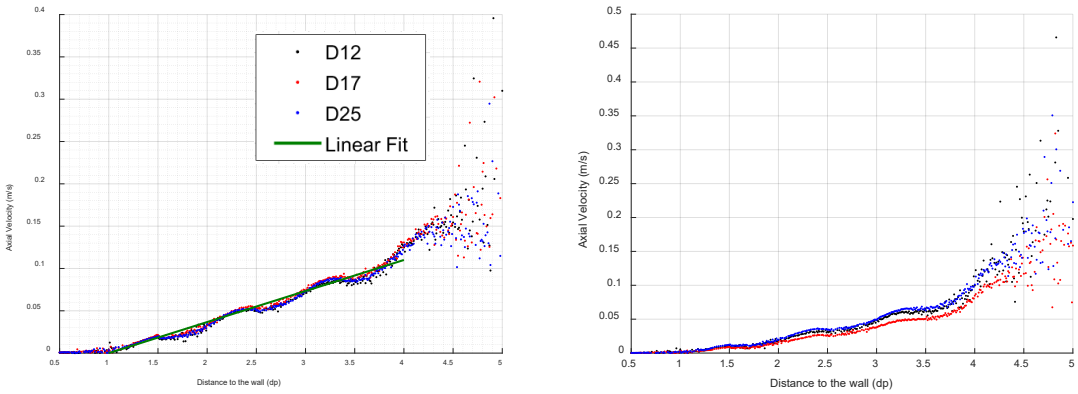


**(a)** **(b)**

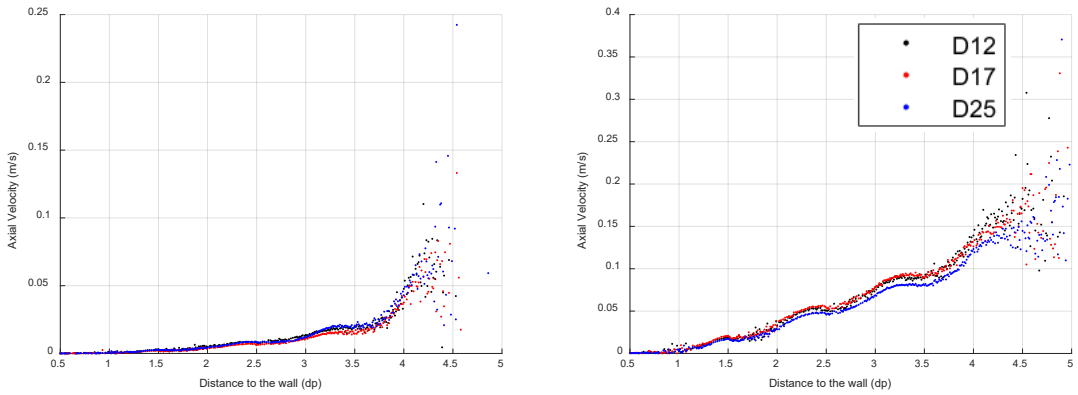


**(c)** **(d)**

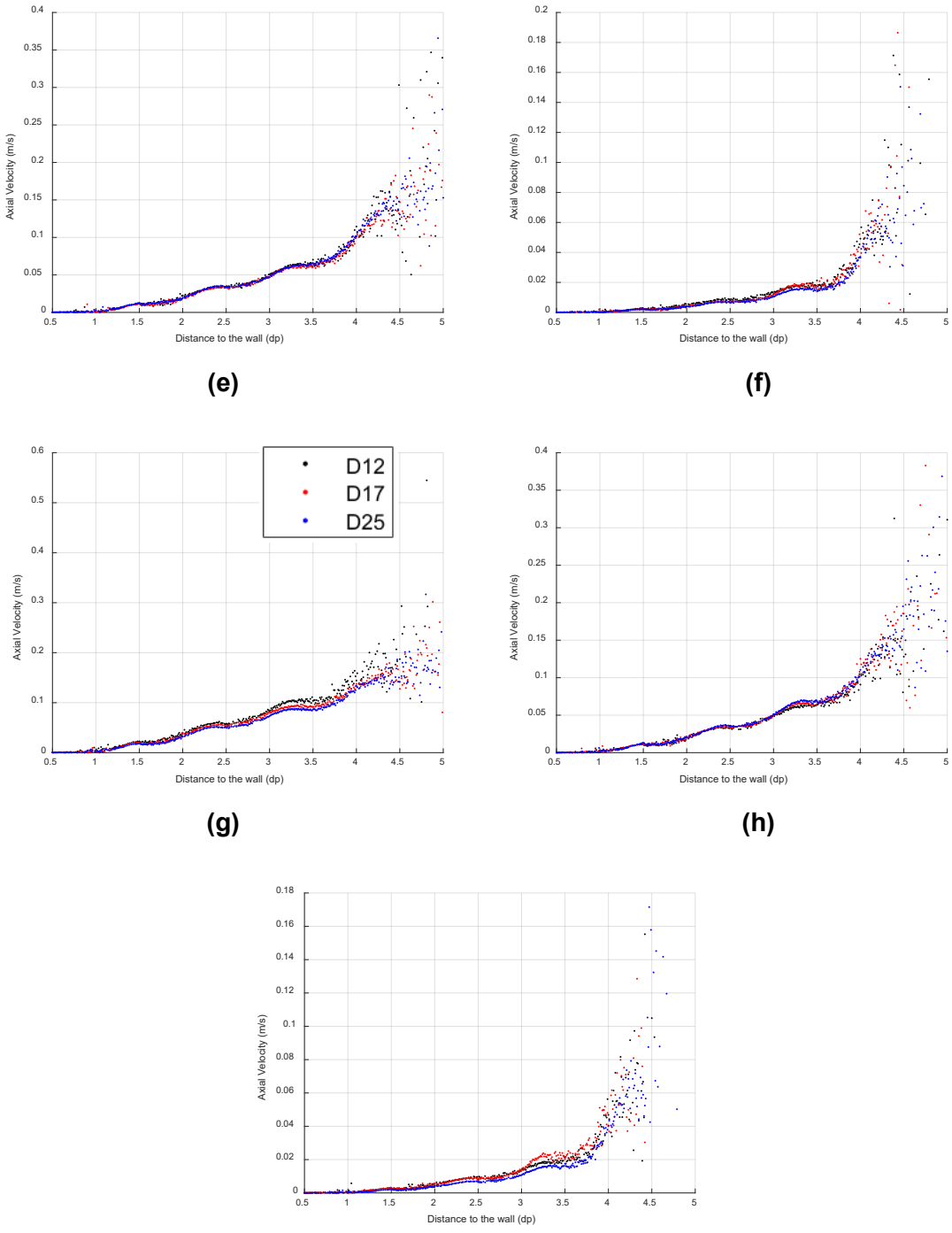


**Figure 6.** Axial velocity profile in radial direction at non-dimensional axial position of z = 0.3 for tangential position of (a) 45° (b) 90° and (c) 135°, z = 0.5 (d)-(f), z = 0.7 (g)-(i).

## 5. Conclusion

In this study, a scale down approach for CentRec is proposed and validated. The results show that the velocity profile and film thickness distribution can be predicted for large scale receivers by running DEM simulations for a scaled-down size. As a next step, the developed approach will be coupled to developed thermal model [6] to derive the effective thermal conductivity of moving particle film for various operation conditions.

## Author Contributions

**Serdar Hicdurmaz:** Conceptualization, Methodology, Writing. **Reiner Buck:** Review & Editing, Supervision, Funding acquisition. **Bernhard Hoffschmidt:** Supervision, Funding acquisition.

## Competing Interests

The authors declare that they have no competing interests.

## Funding

The authors acknowledge the financial support of DLR-DAAD Research Fellowship Programme.

## References

1. W. Wu, "A centrifugal particle receiver for high-temperature solar applications," Ph.D. Thesis, RWTH Aachen University, Aachen, Germany, 2014.
2. S. Hicdurmaz, E. Johnson, J. Grobbel, L. Amsbeck, R. Buck, and B. Hoffschmidt, "Numerical Heat Transfer Modelling of a Centrifugal Solar Particle Receiver (accepted)," presented at the SolarPACES, Virtual Conference, September 28 - October 2, 2020. https://doi.org/10.1063/5.0086375
3. S. Hicdurmaz, J. Grobbel, R. Buck, and B. Hoffschmidt, "A numerical radiation model for the centrifugal particle solar receiver," in *AIP Conference Proceedings*, Virtual, Online, September 27 – October 1 2021: AIP Conference Proceedings. (accepted)
4. J. Grobbel, "Modeling Solar Particle Receivers with the Discrete Element Method," Ph.D. Thesis, RWTH Aachen University, Aachen, Germany, 2019. 10.18154/RWTH-2020-01764
5. "LIGGGHTS(R)-PUBLIC Documentation, Version 3.X." https://www.cfdem.com/media/DEM/docu/Manual.html (accessed 2022).
6. S. Hicdurmaz, "Numerical and Experimental Investigation of Centrifugal Solar Particle Receiver," Ph.D. Thesis, RWTH Aachen University, 2023. (Under Review)
7. J. Grobbel, S. Brendelberger, M. Henninger, C. Sattler, and R. Pitz-Paal, "Calibration of parameters for DEM simulations of solar particle receivers by bulk experiments and surrogate functions," *Powder Technology,* vol. 364, pp. 831-844, 2020, doi: https://doi.org/10.1016/j.powtec.2019.11.028.
8. S. Hicdurmaz, R. Buck, and B. Hoffschmidt, "Image Analysis of Particle Flow in Cent rifugal Solar Particle Receiver," in *Energy Sustainability*, Virtual, Online June 16–18, 2021 2021: ASME, https://doi.org/10.1115/ES2021-63763